Numerical and experimental study of the effects of WEC motion on a combined wind-wave energy platform

Hongbhin Kim and Weoncheol Koo

Abstract—**In this study, the motion response of a combined wind-wave energy platform equipped with multi wave energy converters (WEC) that can control the motion of a floating offshore wind turbine (FOWT) was analyzed numerically and verified through a two-dimensional mini wave tank experiment. The combined energy platform attaching the WEC to the FOWT not only produces stable energy by controlling the motion of the FOWT with the motion of the WEC, but also produces wave energy by the relative motion of the WEC. The FOWT is a taut mooring spar-type platform, and the WEC is a moving cylinder hinged to the FOWT. The motion reduction effect of the FOWT by the motion of the WEC was analyzed. Numerical analysis used a potential flow-based hydrodynamic program (AQWA). To estimate the restraining force of the FOWT due to the motion of the WEC, the multibody dynamics theory was applied, and the accuracy of the numerical model was improved by applying mooring dynamics, weakly nonlinear Froude-Krylov force, and nonlinear hydrostatic force. The experimental model was fabricated on a scale of 1/100 of the numerical model and was performed in a two-dimensional mini wave tank. The numerical analysis results were in good agreement with the experimental results. In particular, the pitch of FOWT by the motion of WEC significantly decreased near the pitch resonance area. Using the verified numerical model, the behaviour of the combined energy platform due to the motion of the WEC under various wave conditions was analyzed in detail.**

Keywords—**Floating offshore wind turbine, Mini wave tank, Model test, Motion response, Wave energy converter**

I. INTRODUCTION

To mitigate the impact of global climate change due to excessive carbon dioxide emissions, it is essential to develop eco-friendly carbon-free ocean energy [1], [2]. Among them, offshore wind is growing as a representative renewable energy source based on the advantage that it can produce a large amount of energy compared to other renewable energy sources [3]. Additionally, a Floating Offshore Wind Turbine (FOWT) has the advantage of being free from noise pollution compared to an onshore wind turbine, and it can produce energy using more stable and stronger winds [4], [5]. Based on these advantages, many European countries including the United Kingdom (UK) and Denmark are actively developing FOWT technologies [6]. In particular, the UK operates large wind farms such as HORNSEA [7] and produces significant amounts of wind energy.

In marine environments with abundant wind resources, the possibility of utilizing abundant wave energy can also be considered [8]. Based on these characteristics, various studies have been conducted on combined wind-wave energy platforms. A combined wind-wave energy platform can increase the economic efficiency by utilizing both energy sources [9] and improve the quality of the energy produced [5], [10]. Furthermore, the combined energy platform has the advantage of increasing the inematic stability of FOWTs [11]. With these features, various combined energy platforms have been developed based on semi-submersible, tension-leg platform (TLP), and Spar type platforms [12].

For the study of combined energy platforms based on semi-submersible FOWTs, numerical and experimental studies have been conducted based on a semi-submersible wind energy platform and flap-type wave energy converter (SFC) model reported through the MARINA project [13]. In addition, a semi-submersible FOWT-based combined energy platform has been demonstrated through projects such as Mermaid [14].

In the study of combined energy platforms based on TLP type platforms, numerical and experimental studies have been conducted on a model with a torus-shaped wave energy converter (WEC) attached to a TLP-shaped FOWT [8].

Research on the combined energy platform based on Spar type FOWT is also being actively conducted. Through the MARINA project, a Spar-torus combination (STC) model with a torus-shaped WEC attached to the FOWT was disclosed [15], and numerical and experimental studies have been conducted on this model [16]. In addition, various combined energy platforms based on Spar FOWTs have been disclosed and studied

©2023 European Wave and Tidal Energy Conference.

H. B. Kim and W. C. Koo are with the Department of Naval Architecture and Ocean Engineering, INHA University, Incheon, Republic of Korea (1st author e-mail: hymdrj@gmail.com, 2nd author (corresponding author) e-mail: wckoo@inha.ac.kr).

Digital Object Identifier: https://doi.org/10.36688/ewtec-2023-192

[17], [18].

The previous studies have mainly focused on numerically and experimentally analyzing the characteristics of wind-wave combined energy platforms. In particular, comparative studies with single wind power platforms have not been carried out to better understand the effects of wave energy converter motion.

In this study, the dynamic response characteristics of the single model and the combined model were analyzed in detail through experiments and numerical simulations to understand the specific effects of wave energy converter attachment on a wind power platform.

The motion analysis of the combined energy platform based on the Spar FOWT was performed numerically and experimentally. Two WECs were hinged to the FOWT, and the motion changes of the FOWT due to the movement of the WECs were analyzed according to various wave periods in a regular wave environment. In addition, the motion performance of the FOWT according to the presence or absence of WEC was investigated.

To accurately analyze the primary effects of the attachment and motion of the WECs on the FOWT, the power take-off (PTO) was not considered, and the effects of the wind tower and turbine were not considered. This study is a preliminary study for an integrated analysis that considers both the effects of wind turbines and the PTO of WECs, and a more precise analysis will be conducted in future studies.

The experiments were performed in a two-dimensional mini wave tank at Inha University, and the numerical analysis was performed using the AQWA time domain analysis program (AQWA-NAUT). To improve the accuracy of the numerical model, nonlinear incident waves [19] and hydrostatic forces were considered, and multibody dynamics techniques were applied to consider the reaction forces acting on the FOWT due to the movement of the WECs. The numerical results were compared with the experimental data for a model that did not consider the mass of the FOWT tower. Finally, the verified numerical model was used to calculate the motion of the combined energy platform for the model including the mass of the wind tower.

II. EXPERIMENTAL MODEL

The model used in this study is shown in Fig. 1. The point-absorber type WECs were attached to the Spar type FOWT and the two WECs are capable of only one-dimensional rotational motion. Four taut mooring lines were attached to the FOWT. The mooring lines were implemented through steel tension springs. Since the buoyancy is greater than the weight of the floating body, there is an initial tension in the mooring lines. Also, as mentioned earlier, to accurately capture the change in response of the FOWT due to the motion of the WEC, the model did not consider the PTO of the WEC and excluded the mass of the wind tower and turbine. The combined energy platform was constructed based on the model proposed by MARINTEK [17] with reference to Hywind Spar [20] and Wave-star [21].

The experimental model was designed at a scale of 1/100 of the prototype model (using Froude scale) in consideration of the size (0.3 m × 6 m × 0.5 m) of the two-dimensional mini wave tank at Inha University, and its main specifications are described in Table 1. The overall view of the experimental model setup is shown in Fig. 2.

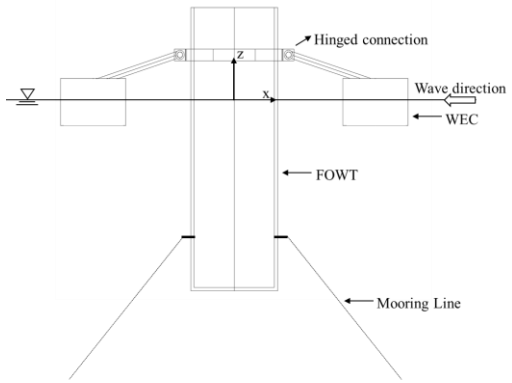

Fig. 1. Model configuration of a combined wind-wave energy platform.

TABLE I
MAIN PARAMETERS OF THE COMBINED WIND-WAVE ENERGY PLATFORM

Parameter	Scaled (1/100)
FOWT part	
Water Depth (m)	0.35
Diameter (m)	0.08
Draft (m)	0.16
Freeboard (m)	0.08
Mass (kg)	0.23
Centre of gravity (m)	-0.0447 (SWL)
Moment of inertia (Roll) (kg·m²)	0.00230
Moment of inertia (Pitch) (kg·m²)	0.00230
Moment of inertia (Yaw) (kg·m²)	0.00034
Ballast mass (kg)	0.34
Mooring system type	Taut mooring
Number of mooring lines	4
Mooring connected position (m)	-0.1 (SWL)
Unstretched mooring line length (m)	0.21
Mooring line stiffness (N/m)	10
Mass per unit length (kg)	0.00071
WEC part	
Draft (m)	0.02
Freeboard (m)	0.02
Hinge-connected position (m)	0.04 (SWL)
Mass (kg)	0.05
Moment of inertia (kg·m²)	0.00003

The overall setup of the experiment is shown in Fig. 3. A piston-type wavemaker was used to generate regular waves, and an ultrasonic wave gauge (TSPC-30S2, SENIX) was used to measure the incident wave height. The wave gauge was installed 1.2 m in front of the combined platform. The movements of the FOWT and WEC were precisely measured using four OPTITRACK Prime 13 motion capture cameras. The wave absorbing system was installed at the end of the wave tank to prevent reflected waves, which was validated by Jung and Koo [22].

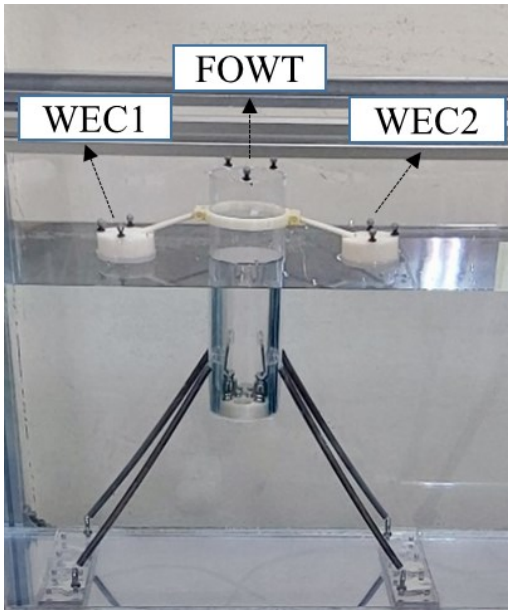

Fig. 2. 1/100 scaled experimental model, WEC 1 is located on the leeside, and WEC2 is located on the weather side.

III. NUMERICAL MODEL

The numerical analysis was performed based on the full scale model. The numerical model used the frequency domain hydrodynamic program (AQWA-LINE) to calculate the hydrodynamic coefficients, considering the interaction between the FOWT and WEC. Then, the time domain analysis was performed using the AQWA-NAUT program. The AQWA-NAUT program can calculate the nonlinear Froude-Krylov force and nonlinear hydrostatic pressure of the FOWT and WEC, and the reaction force due to the dynamic interaction between the FOWT and WEC. The final equation of motion of the FOWT is given by

$$(m + m_a)\ddot{x} = F_{EX} + F_R + F_S + F_M + F_{cons} + F_{vis} \quad (1)$$

where m and m_a denote mass and added mass of the FOWT, respectively. $\ddot{x}$ denotes the acceleration of the FOWT. F_{EX} represents the first-order wave excitation force acting on the FOWT and F_R represents the radiated wave force. F_{STIFF} and F_M denote the restoring force and the force due to the dynamics of mooring lines, respectively. F_{cons} is the constraint force acting on the FOWT due to the motion of the WEC. F_{vis} indicates the viscous damping force. A brief description of each force is given below.

Using the incident wave potential (φ_O) and diffracted wave potential (φ_D), the first-order wave excitation force of the floating body is calculated through the unsteady Bernoulli equation.

$$F_{EX}^1 = -i\omega\rho \iint_{s_b} (\varphi_O + \varphi_D) n_i \, dS \quad (2)$$

where ρ is water density, n denotes normal vector on the body surface and subscript i denotes each motion mode. The radiated wave force is calculated as an impulse response function in the form of convolutional integration that implements the memory effect. $\ddot{x}(\tau)$ refers to the acceleration of the body at time τ and the acceleration impulse response function is equal to $R(t)$. In this case, B(ω) indicates the radiation damping coefficient.

$$F_R = -\int_0^t h(t-\tau) * \ddot{x}(\tau)\, d\tau \quad (3)$$

$$h(t) = \frac{2}{\pi}\int_0^\infty B(\omega)\frac{sin(\omega t)}{\omega} d\omega \quad (4)$$

The restoring force of the FOWT is expressed as the sum of the hydrostatic force ($k_{hydrostatic} * x$) and the

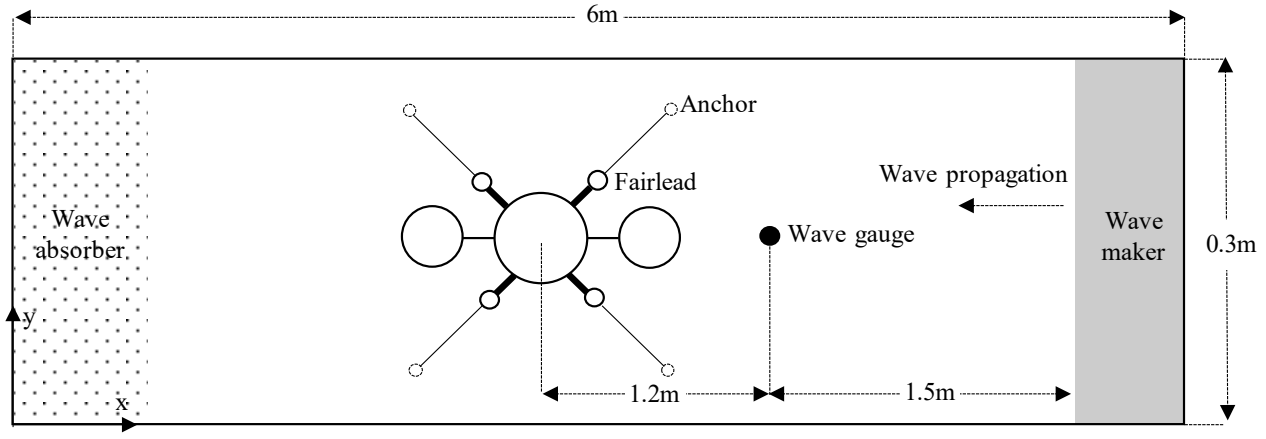

Fig. 3. Plan view of the experimental set-up.

mooring force ($k_{mooring} * x$). x represents the displacement of the body.

$$F_{STIFF} = -(k_{hydrostatic} + k_{mooring}) \times x \quad (5)$$

The force and moment acting on the platform through mooring dynamics can be expressed by the following equations [23]. $[K^L]$ and $[\tilde{P}]$ represent the linear stiffness matrix and translational matrix between FOWT and mooring line, respectively. $[K^\theta]$ and $[\tilde{R}]$ represent the rotational stiffness and motion matrix between FOWT and mooring line, respectively. $[\tilde{C}]$ and $[\tilde{D}]$ represent the translational and rotational motions of the FOWT.

$$F_{M/translation} = -[K^L][\tilde{P}] \quad (6)$$

$$F_{M/moment} = [K^L][\tilde{P}][\tilde{C}] + [K^\theta][\tilde{R}][\tilde{D}] \quad (7)$$

The FOWT and WEC are connected by a hinge joint, and the FOWT can be affected by the movement of the WEC. The constraint force (F_{cons}) has a significant effect on the behavior of the FOWT. The equation for the constraint force F_{CONS} at the hinge joint is shown in (8) [24]. F_j and F_k refer to the total force and moment acting on the FOWT and WEC (excluding the reaction force component), respectively. U_j and U_k denote the 6-DOF motions of FOWT and WEC, respectively. $\begin{bmatrix} K_{jj} & K_{jk} \\ K_{kj} & K_{kk} \end{bmatrix}$ means the total stiffness matrix of FOWT and WEC. H means the boundary condition matrix according to the type of constraints. E is the unit vectors at hinge joints and R_j is the relative vector between the hinge joint and FOWT, and R_k is the relative vector between the hinge joint and WEC. G means the boundary condition matrix to define the hinge condition [24].

$$\begin{bmatrix} K_{jj} & K_{jk} & -H_j^T \\ K_{kj} & K_{kk} & H_k^T \\ H_j & -H_k & 0 \end{bmatrix} \begin{bmatrix} U_j \\ U_k \\ F_{cons} \end{bmatrix} = \begin{bmatrix} F_j \\ F_k \\ 0 \end{bmatrix} \quad (8)$$

$$H_j = \begin{bmatrix} E^T & E^T R_j \\ 0 & G^T \end{bmatrix}, \qquad H_k = \begin{bmatrix} E^T & E^T R_k \\ 0 & G^T \end{bmatrix} \quad (9)$$

IV. COMPARISON OF RESULTS

The results were divided into three parts. First, the experimental data of the single FOWT (no WEC) and the combined energy platform were compared with numerical results. Second, the dynamic response of the combined platform according to the hinged and fixed constraints of the WEC was compared. Finally, using a validated numerical model, the numerical motion response of the single FOWT and the combined platform with tower masses was compared.

TABLE II
INCIDENT WAVE CONDITIONS FOR REGULAR WAVE TEST

Wave Period	Wave Height
0.5 s	0.007 m
0.6 s	0.0126 m
0.7 s	0.0156 m
0.8 s	0.0154 m
0.9 s	0.0124 m
1.0 s	0.0148 m
1.1 s	0.0152 m
1.2 s	0.0156 m

A. *Comparison of experimental and numerical results of FOWT and WEC motions*

The regular wave conditions used in the experiment are described in Table 2. The propagation direction of the incident wave was the negative surge direction (-x). In addition, all results were expressed on an experimental scale. Fig. 4 shows the time series comparison of the experimental data and numerical simulations of the respective motion responses at the resonance period (0.9 s) of the single FOWT. All the responses of surge, heave, and pitch of the single FOWT were in good agreement. Nevertheless, a small error occurred in the heave motion (Fig. 4(b)) in the process of installing a relatively small single FOWT model and conducting the experiment.

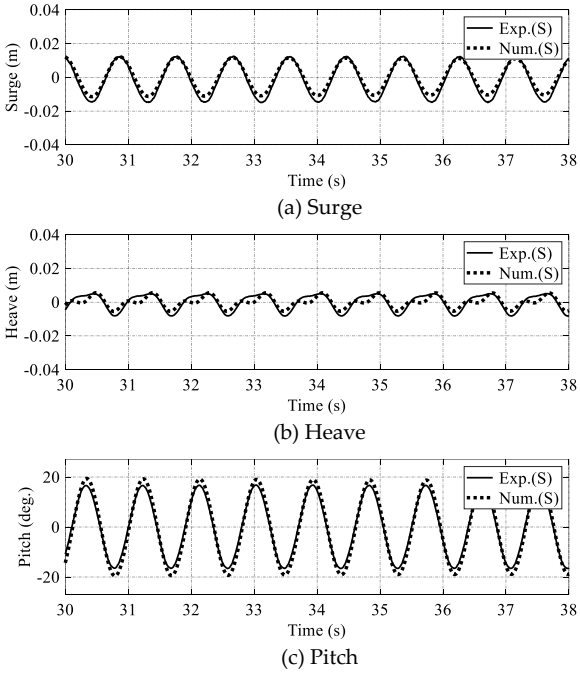

(a) Surge
(b) Heave
(c) Pitch

Fig. 4. Comparison of experimental and numerical results for the motion of a single FOWT (H = 0.0124 m, T = 0.9 s).

Fig. 5 shows the comparison of experimental and numerical results for RAOs of the single and combined energy platforms. As can be seen through the time series data in Fig. 4, the RAO calculations for both numerical and experimental results used the response amplitude

measured in the steady section of 25 to 35 periods, excluding the initial transient section.

For all motion responses, the experimental data and numerical simulations generally agreed well. As mentioned in the numerical model, the nonlinear Froude-Krylov force and the nonlinear hydrostatic force were applied to the numerical model, and the coupling analysis between the FOWT and the mooring lines was considered. This improved the accuracy of the numerical model results. In addition, since the FOWT model is composed of a circular cylinder and the effect of fluid viscosity is relatively small, the results of the potential flow-based numerical simulation are in good agreement. On the other hand, the use of a validated experimental equipment [22] and a high-performance motion camera enabled precise experimental results to be derived.

Comparing the surge RAOs (Fig. 5(a)), the maximum displacement of the single FOWT within a given wave period occurred at 0.9 s, while the maximum displacement of the combined platform occurred at 1.1 s. This was due to the influence of pitch resonance period shown in Fig. 5(c).

The heave RAO of the single FOWT (Fig. 5(b)) showed large displacements at 0.65s and 0.9s. The large displacement at 0.65s is due to the resonant period of heave, and the displacement at 0.9 s is due to the resonant period of pitch. The heave of the combined energy platform with WECs decreased in all periods. However, at longer periods, the heave responses of the two platforms were almost identical.

The pitch RAO of the single FOWT (Fig. 5(c)) showed the largest displacement due to the resonance at 0.9 s, but it decreased sharply for the combined energy platform. This is due to the attachment of the WEC, which shifted the resonance period to 1.1s. In addition, the pitch response of the combined energy platform decreased for all incident wave periods except the pitch resonance period of the combined platform. This shows that the effect of WEC attachment is more pronounced in the pitch response compared to the surge and heave motions.

Fig. 6 compares the experimental and numerical results for the pitch RAO of WEC 1 (leeside) and WEC 2 (whether side). The experimental and numerical values were in good agreement. At the pitch resonance period (1.1 s), the numerical results were slightly larger than the experimental data, which may have been affected by the pitch resonance period of the FOWT. In addition, the WEC motion on the leeside was larger than that on the weather side due to the relatively long period wave (1.1 s). The numerical results showed a similar magnitude of the motion response at all periods.

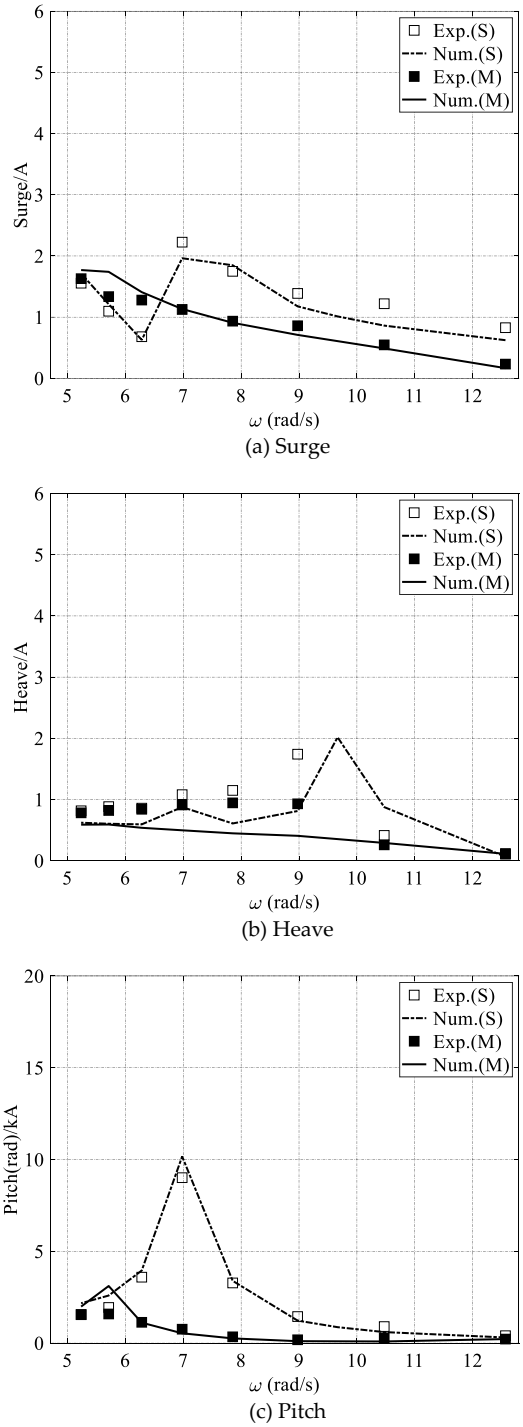

Fig. 5. Comparison of RAOs of the single and combined energy platforms between experimental and numerical results. S denotes the single FOWT. M denotes the combined energy platform. A denotes wave amplitude. k denotes wave number.

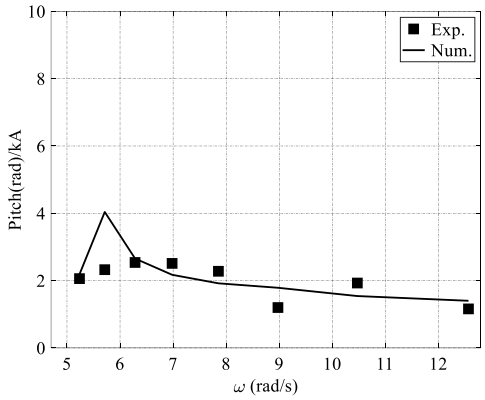

(a) WEC1 (leeside)

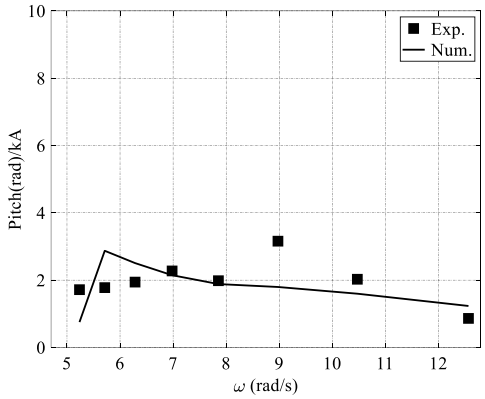

(b) WEC2 (weather side)

Fig. 6. Comparison of Pitch RAO of WEC on the combined energy platform. A denotes wave amplitude. k denotes wave number.

B. *Comparison of motion responses of FOWT according to WEC connection types*

Fig. 7 compares the motion responses of the FOWT according to the connection type of the WEC connected to the combined energy platform. The heave and pitch resonance periods of the combined energy platform were shortened when the WEC was fixed to the platform. This caused all motion responses to be larger at shorter wave periods compared to the hinged connection. For all wave periods, the heave response of the combined energy platform was smaller when the WEC was hinged, and the pitch response showed a sharp decrease when the WEC was hinged, except for the long period waves. However, for long period incident waves, the responses of surge and pitch became larger in the hinged condition. As a result, all the motion responses of the combined energy platform were smaller compared to the single FOWT regardless of how the WECs were connected, meaning that the main cause of the motion reduction of the platform was due to the attachment of the WECs, while the pitch response was reduced more when the WECs were connected in the hinged condition.

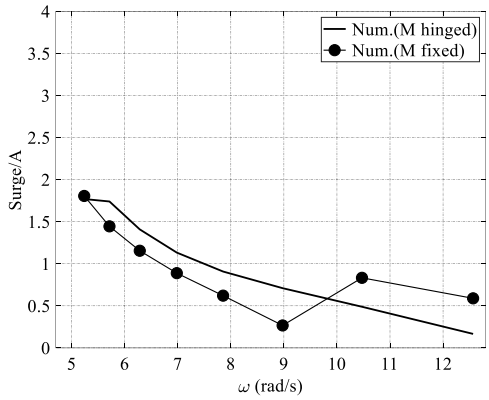

(a) Surge

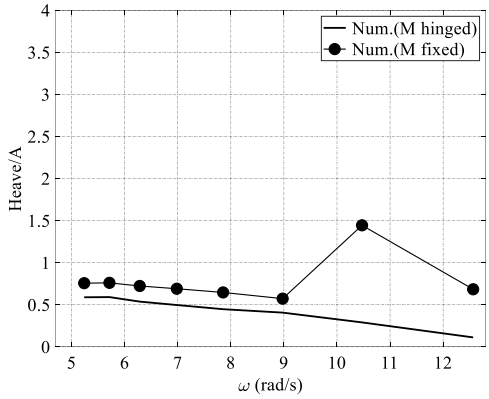

(b) Heave

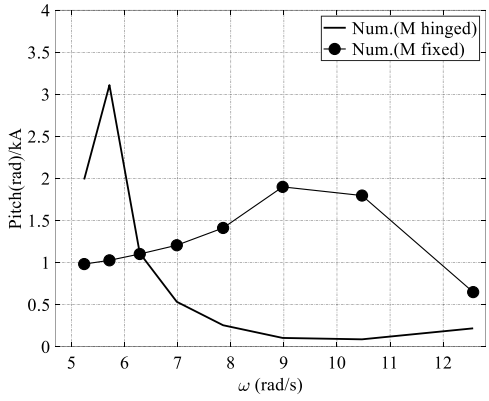

(c) Pitch

Fig. 7. Comparison of motion RAOs of the combined platform according to the connection method of WECs.

C. *Comparison of the motion of the platform including the tower mass*

Using the numerical model verified in Fig. 5, NREL's 5MW wind turbine model was attached to the upper part of the platform and the motion response of the platform was calculated. Both the single FOWT and the combined energy platform with hinged WECs have the same wind turbine specifications, and the total mass of the entire FOWT is the same as the FOWT without the wind turbine through the adjusted ballast mass.

The surge, heave, and pitch responses of the two platforms were compared under the condition of a regular wave of 0.9 s, which is the pitch resonance period of the single FOWT (Fig. 8). The attachment of the wind turbine lengthened the pitch resonance period of the

platform, resulting in a smaller motion response compared to the model without the wind turbine. In addition, the pitch response of the combined energy platform with the WEC attached was significantly reduced compared to the single FOWT.

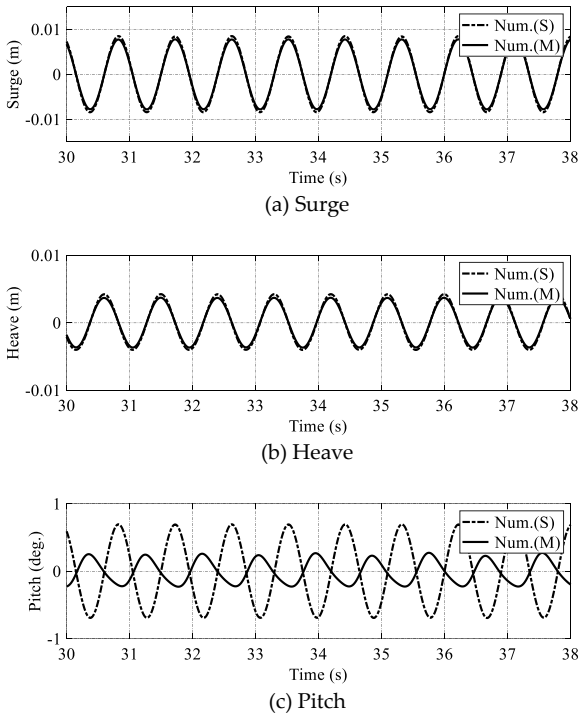

(a) Surge

(b) Heave

(c) Pitch

Fig. 8. Comparison of motion of the platform including tower mass (H= 0.0142 m, T= 0.9 s).

V. CONCLUSION

In this study, the motion responses of a single Spar-type FOWT and a FOWT with two WECs attached (combined energy platform) was analyzed through experiments and numerical analysis. The effects of the wind tower and PTO were excluded to accurately determine the effects of the WEC motions.

The experimental and numerical results were in good agreement, and the overall motion of the combined energy platform was reduced due to the attachment of the WEC, especially the pitch response was significantly reduced.

The motion of the combined energy platform was further reduced when the WECs were hinged, but even when the WECs were fixedly attached, the motion was still less than that of a single FOWT. Therefore, it is confirmed that the reduced platform motion was more influenced by the attachment of WECs. Using a validated numerical model, the motion reduction due to the attachment of WECs was also confirmed in a FOWT model with a wind tower.

Considering the effects of WEC analyzed in this study, the motion characteristics of the combined energy platform with wind tower, WEC attachment, and PTO effects will be focused on through wave tank experiments and time-domain numerical analysis. Given that the aerodynamic forces acting on the wind turbine increase the pitch motion of the tower, the attachment of the WEC will help improve the dynamic stability of the entire platform, and future research will apply aerodynamic calculation programs to analyze these effects in more detail. In addition, the motion characteristics of the combined platform under irregular wave conditions will be analyzed.

ACKNOWLEDGEMENT

This research was funded and conducted under the Competency Development Program for Industry Specialists of the Korean Ministry of Trade, Industry and Energy (MOTIE), operated by KIAT (No. P0012646). This work was also partly supported by the National Research Foundation of Korea (NRF) grant funded by the Korea government (MSIT) (2018R1D1A1B07040677)

REFERENCES

[1] S. Astariz and G. Iglesias, "Wave energy vs. other energy sources: A reassessment of the economics," *International Journal of Green Energy*, vol.13, no. 7, pp. 747-755, 2016.

[2] C. Perez-Collazo, R. Pemberton, D. Greaves, and G. Iglesias, "Monopile-mounted wave energy converter for a hybrid wind-wave system," *Energy Conversion and Management*, vol.*199*, pp. 111971, 2019.

[3] B. J. Koo, A. J. Goupee, R. W. Kimball and K. F. Lambrakos, "Model tests for a floating wind turbine on three different floaters," *Journal of Offshore Mechanics and Arctic Engineering*, vol. *136*, no. 2, 2014.

[4] Y. H. Bae and M. H. Kim, "Rotor-floater-tether coupled dynamics including second-order sum–frequency wave loads for a mono-column-TLP-type FOWT (floating offshore wind turbine),". *Ocean engineering*, vol. *61*, pp. 109-122, 2013.

[5] L. da Silva, N. Sergiienko, B. Cazzolato and B. Ding, "Dynamics of hybrid offshore renewable energy platforms: Heaving point absorbers connected to a semi-submersible floating offshore wind turbine," *Renewable Energy*, *vol.199*, pp. 1424-1439, 2022.

[6] GWEC, Global Wind Energy Council. "Global wind report 2022," 2022.

[7] Note, MMO Clarification. "Hornsea Offshore Wind Farm Project One," 2014.

[8] N. Ren, Z. Ma, B. Shan, D. Ning and J. Ou, "Experimental and numerical study of dynamic responses of a new combined TLP type floating wind turbine and a wave energy converter under operational conditions," *Renewable Energy*, vol. *151*, pp. 966-974, 2020.

[9] H. Zhang, N. Zhang, and X. Cao, "Conceptualization and dynamic response of an integrated system with a semi-submersible floating wind turbine and two types of wave energy converters," *Ocean Engineering*, vol. *269*, pp. 113517, 2023.

[10] K. H. Kim, S. Park, J. R. Kim, I. H. Cho, and K. Hong, "Numerical and experimental analyses on motion responses on heaving point Absorbers connected to large semi-submersibles," *Processes*, vol. *9*, no. 8, pp. 1363, 2021.

[11] H. B. Kim, E. H. Min, S. H. Heo, and W. C. Koo, "Motion Analysis of A Wind-Wave Energy TLP Platform Considering Second-order Wave Forces," *Journal of Ocean Engineering and Technology*, vol. *36*, no. 6, pp. 390-402, 2022.

[12] H. R. Ghafari, H. Ghassemi, A. Abbasi, K. A. Vakilabadi, H. Yazdi and G. He, "Novel concept of hybrid wave star-floating offshore wind turbine system with rectilinear arrays of WECs," *Ocean Engineering*, vol. *262*, pp. 112253, 2022.

[13] C. Michailides, Z. Gao and T. Moan, "Experimental and numerical study of the response of the offshore combined wind/wave energy concept SFC in extreme environmental conditions," *Marine structures*, vol. *50*, pp. 35-54, 2016.

[14] M. Colluand and E. E. Bachynski, "Multipurpose platforms," 2019.

[15] M. J. Muliawan, M. Karimirad, T. Moan and Z. Gao, "STC (Spar-Torus Combination): a combined spar-type floating wind turbine and large point absorber floating wave energy converter—promising and challenging," in *International Conference on Offshore Mechanics and Arctic Engineering*, 2012, vol. 44946, pp. 667-676.

[16] L. Wan, M. Greco, C. Lugni, Z. Gao and T. Moan, "A combined wind and wave energy-converter concept in survival mode: Numerical and experimental study in regular waves with a focus on water entry and exit," *Applied Ocean Research*, vol. *63*, pp. 200-216, 2017.

[17] M. Karimirad and K. Koushan, "WindWEC: Combining wind and wave energy inspired by hywind and wave star," In *2016 IEEE International Conference on Renewable Energy Research and Applications*, pp. 96-101, 2016.

[18] H. R. Ghafari, A. Neisi, H. Ghassemi and M. Iranmanesh, "Power production of the hybrid Wavestar point absorber mounted around the Hywind spar platform and its dynamic response," *Journal of Renewable and Sustainable Energy*, vol. 13, no. 3, pp. 033308, 2021.

[19] G. Giorgi and J. V. Ringwood, "Analytical representation of nonlinear Froude-Krylov forces for 3-DoF point absorbing wave energy devices," *Ocean Engineering*, vol. *164*, pp. 749-759, 2018.

[20] F. Driscoll, J. Jonkman, A. Robertson, S. Sirnivas, B. Skaare and F. G. Nielsen, "Validation of a FAST model of the statoil-hywind demo floating wind turbine," *Energy Procedia*, vol. *94*, pp. 3-19, 2016.

[21] R. H. Hansen, M. M. Kramer and E. Vidal, "Discrete displacement hydraulic power take-off system for the wavestar wave energy converter," *Energies*, vol. *6*, no. 8, pp. 4001-4044, 2013.

[22] H. C. Jung and W. C. Koo, "An Experimental Study on Wave Absorber Performance of Combined Punching Plate in a Two-Dimensional Mini Wave Tank," *Journal of Ocean Engineering and Technology*, vol. *35*, no. 2, pp. 113-120, 2020.

[23] Z. Ran, "Coupled dynamic analysis of floating structures in waves and currents," Ph. D. dissertation, Texas A&M University, USA, 2000.

[24] Ansys, "ANSYS AQWA theory manual, release 18.2," 2016.